AFRL-ML-WP-TR-2006-4207

COLLABORATIVE RESEARCH AND DEVELOPMENT

Delivery Order 0041: Models for the Prediction of Interfacial Properties

Bence Bartha

Universal Technology Corporation
1270 North Fairfield Road
Dayton, OH 45432-2600

AUGUST 2006

Final Report for 25 July 2005 – 04 August 2006

Approved for public release; distribution is unlimited.

STINFO COPY

MATERIALS AND MANUFACTURING DIRECTORATE
AIR FORCE RESEARCH LABORATORY
AIR FORCE MATERIEL COMMAND
WRIGHT-PATTERSON AIR FORCE BASE, OH 45433-7750

NOTICE AND SIGNATURE PAGE

This report was cleared for public release by the Air Force Research Laboratory Wright Site (AFRL/WS) Public Affairs Office and is available to the general public, including foreign nationals. Copies may be obtained from the Defense Technical Information Center (DTIC) (http://www.dtic.mil).

AFRL-ML-WP-TR-2006-4207 HAS BEEN REVIEWED AND IS APPROVED FOR PUBLICATION IN ACCORDANCE WITH ASSIGNED DISTRIBUTION STATEMENT.

*//Signature//	//Signature//
RITA SCHOLES	ROBERT ENGHAUSER
Project Manager	Acting Chief
Business Operations Branch	Business Operations Branch
Integration and Operations Division	Integration and Operations Division

*Disseminated copies will show "//signature//" stamped or typed above the signature blocks.

REPORT DOCUMENTATION PAGE

Form Approved
OMB No. 0704-0188

1. REPORT DATE *(DD-MM-YY)*	2. REPORT TYPE	3. DATES COVERED *(From - To)*
August 2006	Final	07/25/2005 – 08/04/2006

4. TITLE AND SUBTITLE
COLLABORATIVE RESEARCH AND DEVELOPMENT
Delivery Order 0041: Models for the Prediction of Interfacial Properties

5a. CONTRACT NUMBER
F33615-03-D-5801-0041

5b. GRANT NUMBER

5c. PROGRAM ELEMENT NUMBER
62102F

6. AUTHOR(S)
Bence Bartha

5d. PROJECT NUMBER
4349

5e. TASK NUMBER
L0

5f. WORK UNIT NUMBER
VT

7. PERFORMING ORGANIZATION NAME(S) AND ADDRESS(ES)
Universal Technology Corporation
1270 North Fairfield Road
Dayton, OH 45432-2600

8. PERFORMING ORGANIZATION REPORT NUMBER
S-531-0041

9. SPONSORING/MONITORING AGENCY NAME(S) AND ADDRESS(ES)
Materials and Manufacturing Directorate
Air Force Research Laboratory
Air Force Materiel Command
Wright-Patterson AFB, OH 45433-7750

10. SPONSORING/MONITORING AGENCY ACRONYM(S)
AFRL-ML-WP

11. SPONSORING/MONITORING AGENCY REPORT NUMBER(S)
AFRL-ML-WP-TR-2006-4207

12. DISTRIBUTION/AVAILABILITY STATEMENT
Approved for public release; distribution is unlimited.

13. SUPPLEMENTARY NOTES
PAO Case Number: AFRL/WS 06-2486, 18 Oct 2006.

14. ABSTRACT (*Maximum 200 words*)
The research in support of the Air Force Research Laboratory, Materials and Manufacturing Directorate was conducted at Wright-Patterson AFB, Ohio from 25 July 2005 through 4 August 2006. The task developed various experimental and computational tools to determine the material behavior of weld interfaces and local grain behavior of materials. Stereo imaging, optical microscopy and scanning electron microscopy were used to determine the local interfacial characteristics of welds as well as microstructural characteristics of grains at a micro-scale. Computational tools were also developed to analyze and combine the tensile and fatigue data for the various applications. The data shows large strain concentrations develop near the weld interface develop for resistance welds, and near grain boundaries of grain interfaces. The combined data shows the heterogeneous behavior of grains on a micro-scale. Semi-analytical computational tools that determine the stress field of two contacting bodies were also used to analyze and publish data for various contact fatigue applications. The results in the publication show the need for accurate stress based modeling tools to predict the fatigue and crack growth behavior of contracting bodies.

15. SUBJECT TERMS
digital image correlation, additive manufacturing, weld modeling, contact mechanics, fretting fatigue

16. SECURITY CLASSIFICATION OF:			17. LIMITATION OF ABSTRACT:	18. NUMBER OF PAGES	19a. NAME OF RESPONSIBLE PERSON (Monitor)
a. REPORT	b. ABSTRACT	c. THIS PAGE			Rita Scholes
Unclassified	Unclassified	Unclassified	SAR	28	19b. TELEPHONE NUMBER *(Include Area Code)* N/A

Standard Form 298 (Rev. 8-98)
Prescribed by ANSI Std. Z39-18

Introduction

The work conducted under Contract F33615-03-D-5801, Task Order 0041 comprised of developing modeling and experimental tools aimed at process performance and mechanical behavior characterization.

Most Air Force equipment has parts that require machining. Any machining process, milling, drilling, sawing, etc. results in deformation and heating of the material adjacent to the cut material. This deformation and heating cause residual stress fields and changes in the microstructure that can be the source of cracking that results in the failure of the part. The effect of cutting conditions such as cutting speed, depth of cut, coolant type and other processing parameters on the machined component must be characterized in order to develop process performance models for machined surfaces. These process performance models can then be used to minimize tensile residual stress fields and microstructural changes that may cause a debit in the material performance.

Determining the local strain field in a material is an important technique that is needed by the Air Force to determine the effect of microstructural properties such as grain size and orientation, as well as the effect of weld applications on the local mechanical properties of a material. The strain field obtained from areas that have been exposed to a weld process can also be used to calculate local mechanical properties of weld interfaces. Digital image correlation techniques can be used to determine such strain fields on a grain scale. These strain mapping techniques need to be developed further using optical microscopy, scanning electron microscopy and stereo imaging in order to characterize the local strain gradients for various materials and applications in the Air Force.

Numerical subroutines that model the stress field between two contacting bodies has been used to characterize contact fatigue problems that arise at the blade-disk interface in aircraft engines. The stress fields can be used to predict the performance of components in contact fatigue. Further development of the numerical subroutines that calculate these contact stresses is needed to account for contacting bodies that have arbitrary geometry, thickness, material properties and loading conditions.

Universal Technology Corporation used models that describe the behavior of metallic materials under contact conditions during operation. The contact conditions ranged from the transient contact seen during operations like machining up to firmly bonded contact found in most welds. The main thrust of this work is broken down into four fundamental areas. These areas are: 1. Fundamental understanding of contact stresses in arbitrary geometries. 2. Development of full-field strain mapping technologies that will enable the determination of strain gradients in the vicinity of various interfaces, 3. Determination of the mechanical properties of various welded interfaces, and 4. Modeling any post-contact residual stress development and associated deformation in machining operations.

1. Weld Interface Study

1.1 Resistance welds

The resistance plug welding process utilizes the resistance welding technique while incorporating an external insert. Instead of attaching two separate pieces of material, the insert mends a hole that has been created in an area on a single piece of material. The process has been developed by the Edison Welding Institute (EWI). EWI has been working a design of experiment (DOE) to establish the effect of the rivet hole size, preheat current, preheat time, weld current and weld time for the insert. The material that was used for the inserts as well as the base material during the analysis is Ti-6Al-4V.

EWI's first task was to develop an insert design that would give desirable results. After experimenting with two designs, Figures 1 and 2, they determined that a tapered insert were the best welds. Design two offered the best possibility of complete fusion between the insert and the plate.

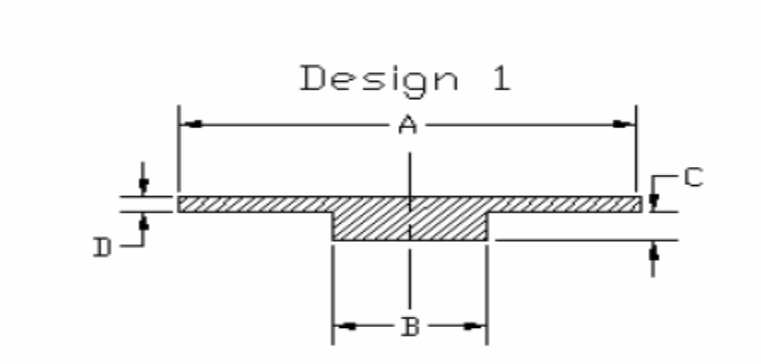

Figure 1: Flat Cononsumable Configuration

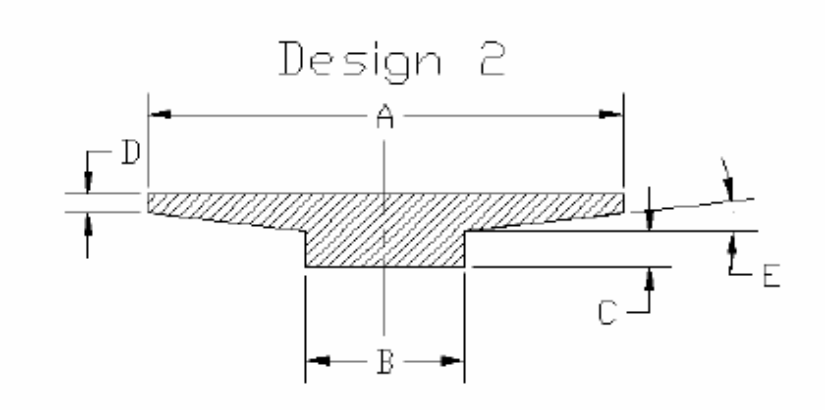

Figure 2: Tapered Cononsumable Configuration

EWI produced samples using the design two insert and examined the specimen for porosity, indentation below the base metal, total crack length, maximum single crack length, maximum pore size, and presence of alpha case. Three hole sizes were used 0.125, 0.156, and 0.187 in. They placed the inserts in the center of the hole and to one side to simulate average and worst case scenario. Their results showed the best welds are

produced at a preheat time of 35 cycles, 1.75-kA preheat current, 10-cycle cool time, 5.0-kA welding current and a 10-cycle weld time.

The in-house effort at AFRL/MLLM included non-destructive inspection (NDI), metallurgical examination, and mechanical testing of a plug-welded sheet. The sheet was mill annealed Ti-6Al-4V, 0.034 in. thick with ten resistance welds plugged at EWI. The NDI and microstructural characterization was performed by Adrieene Schaub, and the AFRL/MLS Systems Support group. Tensile and fatigue testing was performed using a Trilion ARAMIS strain mapping system with stereo imaging capability in conjunction with a 100kip MTS servo-hydraulic machine (Figure 3). White spray-paint was used on the specimen, and a finish black speckle pattern was sprayed on the base to obtain a contrasting pattern ideal for displacement mapping (Figure 4).

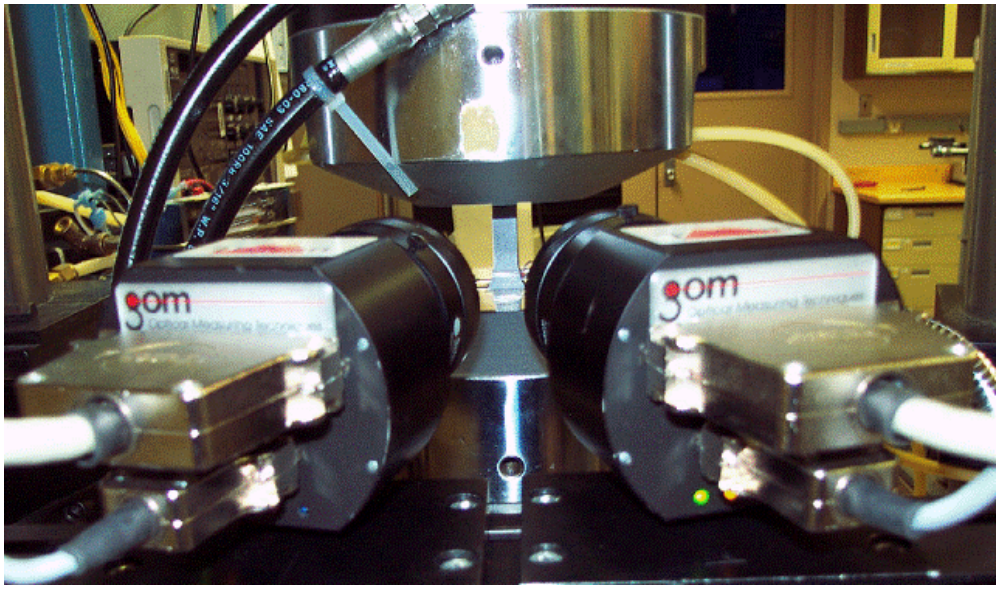

Figure 3: Stereo imaging experimental setup

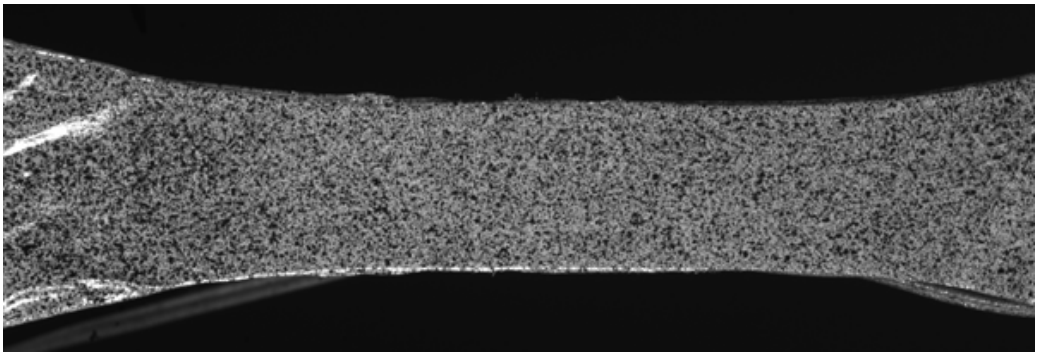

Figure 4: Image showing speckle pattern of stereo imaged sample

1.2 Mechanical Testing Results:

Tensile and fatigue testing was done on the resistance plug welds and on the base metal for comparison. A total of nine ASTM E8 dog bones were mechanically tested. Two base metal dog bones, resistant plug weld 8, and resistant plug weld 10 were tensile tested. One base metal dog bone, resistant plug weld 7 and resistant plug weld 9 were used for the fatigue tests. The base metal fatigue life was 54, 059 cycles. Resistance weld 7 made 33, 930 cycles and resistance weld 9 made 31, 678 cycles. The welds exhibited roughly a 40% reduction in life. The fatigue tests revealed a problem in the repair process.

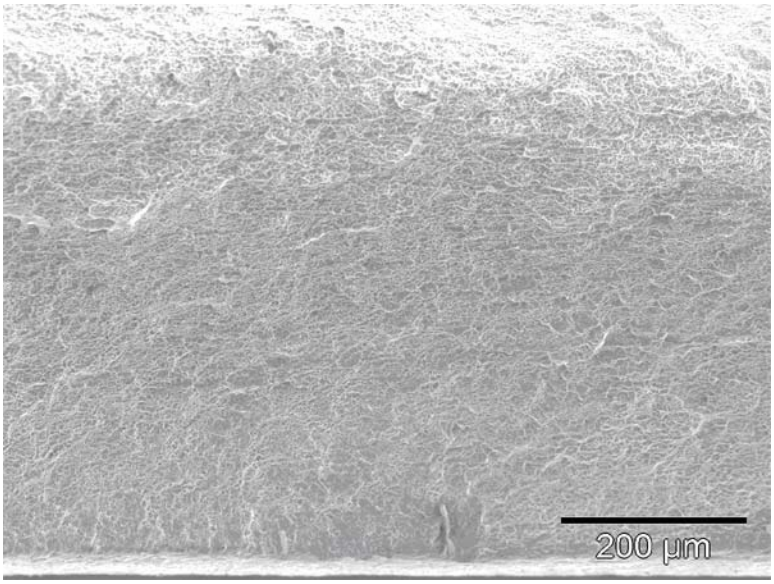

Figure 5: Fracture initiation sight for base metal

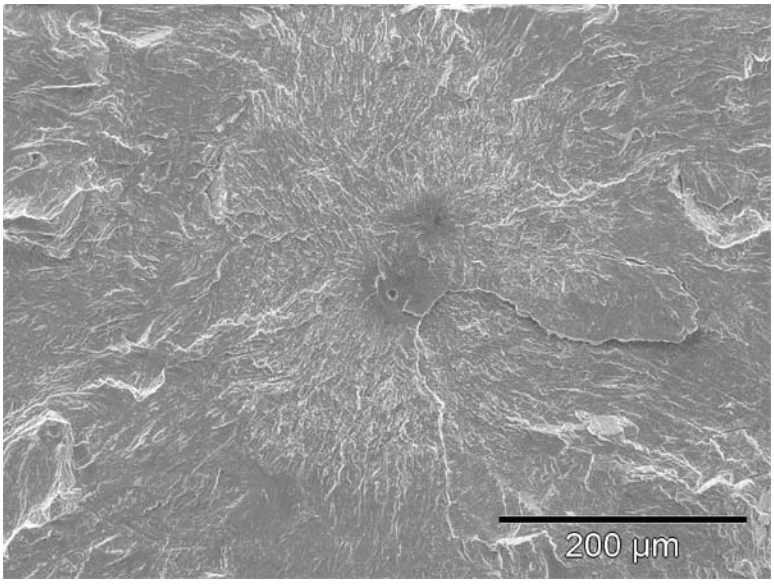

Figure 6: Fracture initiation site for resistance weld 7

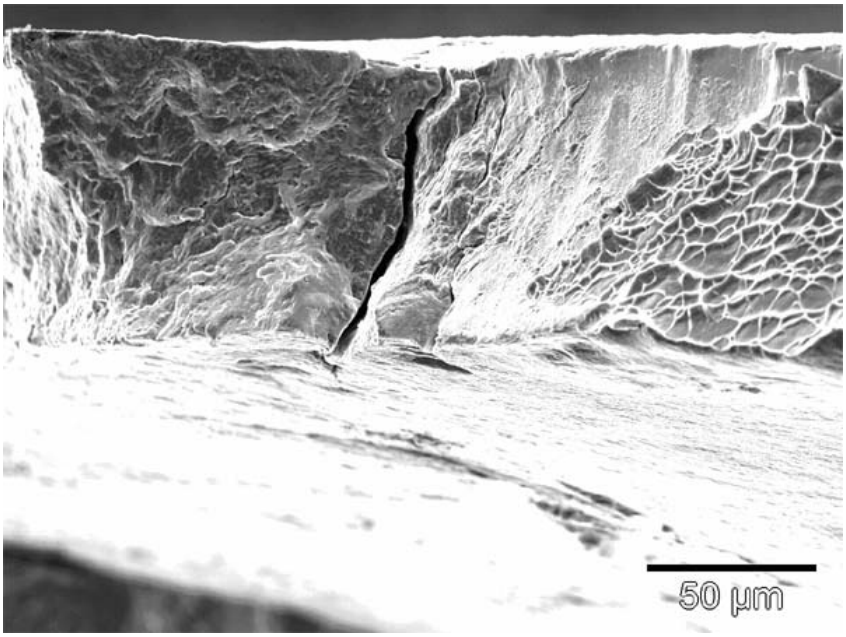

Figure 7: Crack found after fatigue test in resistance weld 7

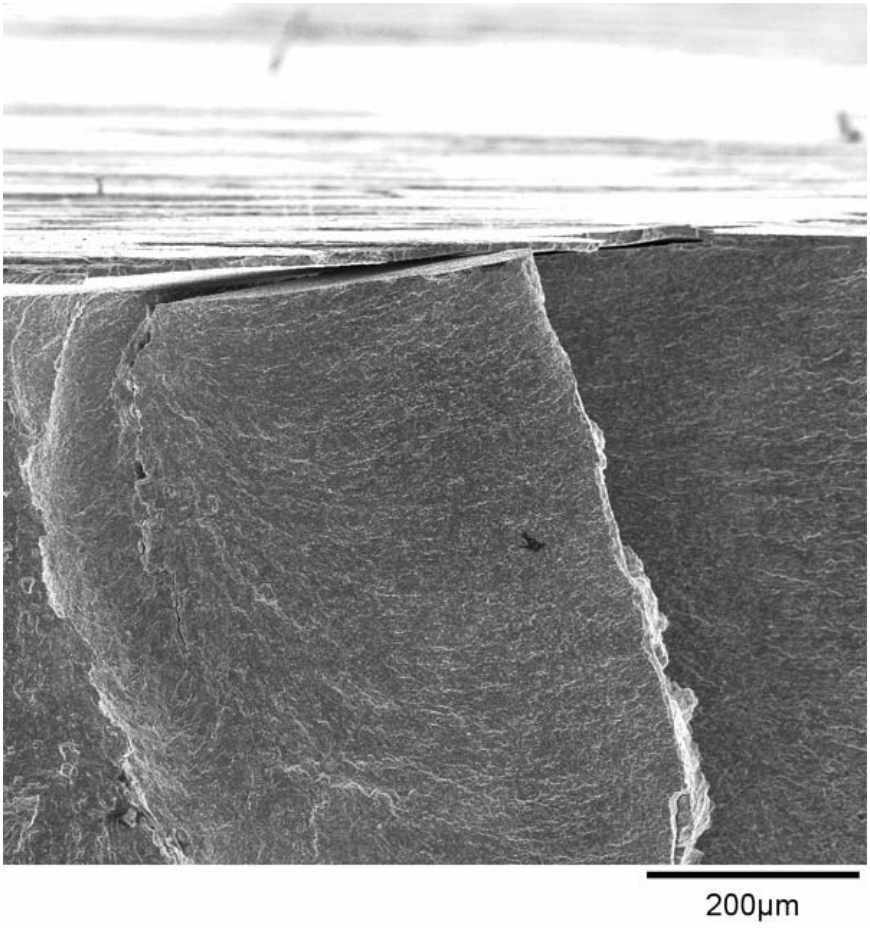

Figure 8: Fracture initiation site for resistance weld 9

After the mechanical testing the surface of some of the specimen were examined to find the fracture initiation points. They were examined using a secondary electron microscope. Figure 5 shows the initiation point in the base metal. It started at some unidentifiable flaw, possibly a spark from the spot welds hit the metal. Figure 6 and 7 are from resistance weld 7. Figure 6 shows the fracture initiation point possibly being a pore. The indication shown in figure 7 is a concern; however, it did not cause the fracture. The fracture initiation point in weld 9 is shown in Figure 8.

The base metal exhibited a tensile strength of roughly 145 ksi (Figure 9). Resistance weld number 10 showed close to the same strength holding 150 ksi (Figure 10). The pressures listed above were the pressures exerted when the sample broke. The tensile test failed resistance weld 10 at a 45^{o} angle. This would suggest that no defect was present and the fracture was due to overload. Post test thickness measurements revealed the sample had significant variations in thickness near the failure location and thus confirmed the hypothesis that the fracture occurred because of necking.

The stress strain curve in Figure 10 shows the strain obtained from the attached strain gage near the weld, and corresponding mean strain measured with optical strain mapping. The two data sets compare well in the elastic regime, and the strain field was obtained in the plastic with the strain mapping. A contour plot in Figure 11 of the axial strain in the plastic regime shows the strain concentration that is occurring near the weld is on the sample where the failure occurred. The strain field confirmed that the failure occurred to the local strain concentration due to the weld.

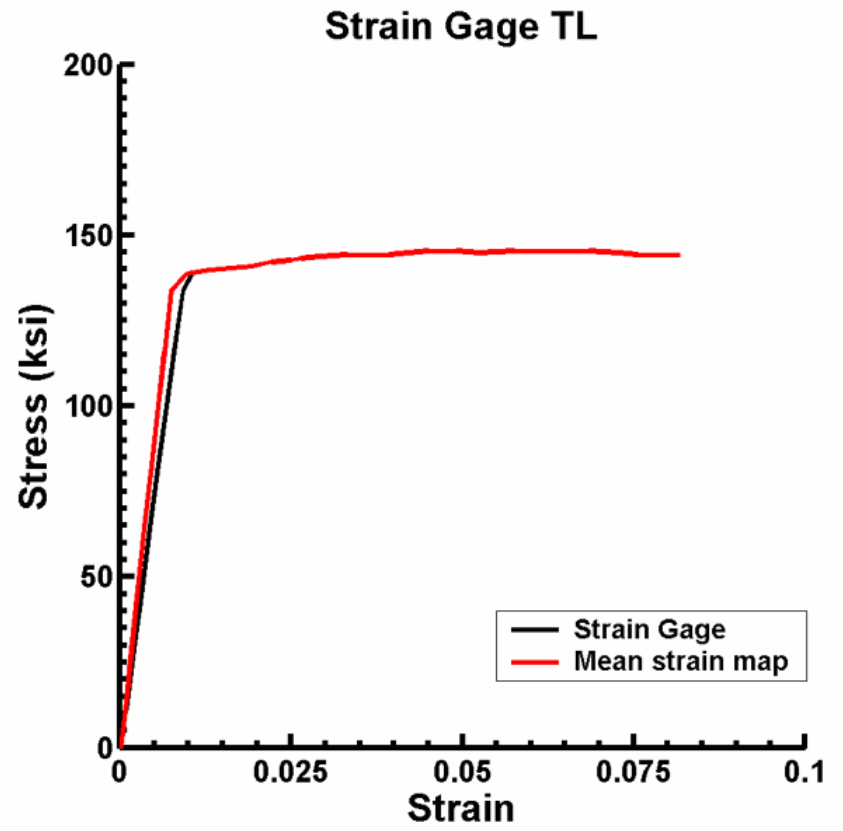

Figure 9: Baseline stress strain curve for the non-welded specimen

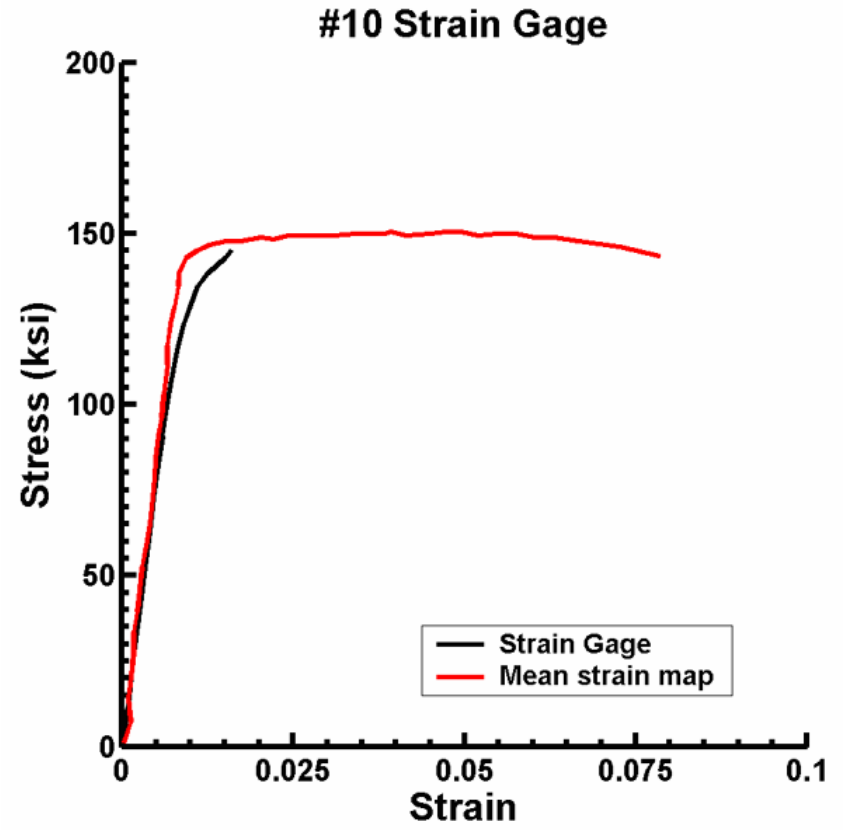

Figure 10: Stress strain curve for tensile test of specimen #10

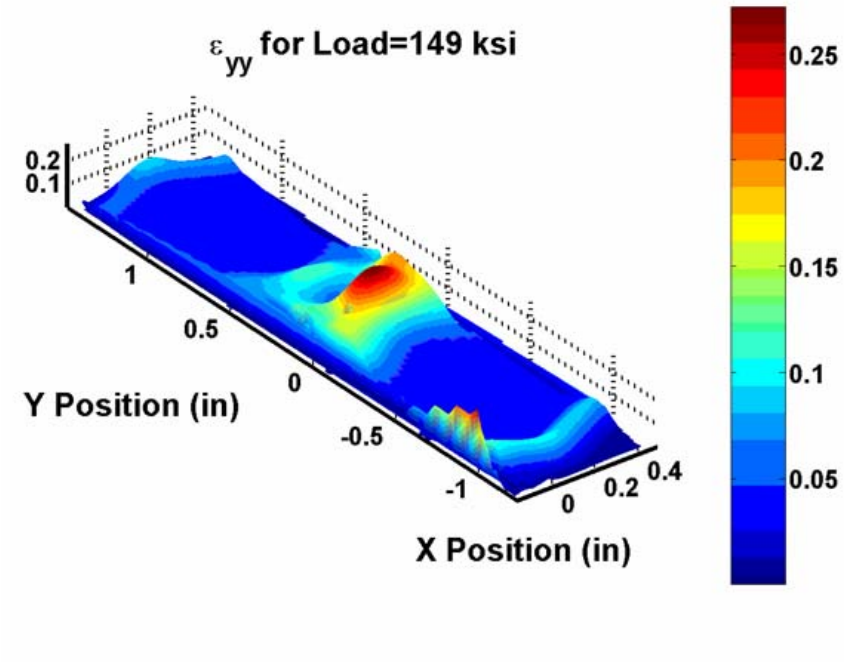

Figure 11: Strain Contour of specimen 10 after yield.

The other resistance weld exhibited a lower strength than the base metal holding 103.69 ksi. This is the stress exerted to break the sample. This weld had indications of lack of fusion of the weld to the base metal on both sides of the weld. These indications are shown in figures 12 and 13. In figure 12 the base metal is on the left and the weld is on the right. There is a dark line to which an arrow is pointing that indicates a lack of fusion. In figure 13 the orientation is reversed. The insert is on the left and the base metal is on the right. The dark line the arrow is pointing to represents a lack of fusion between the two entities.

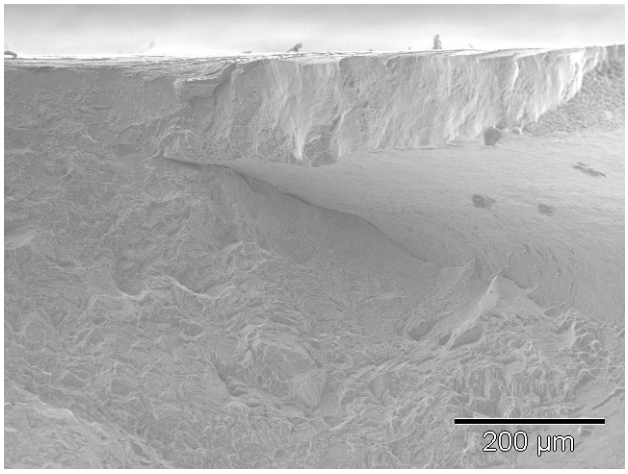

Figure 12: Tensile tested specimen 8 at 150x. Implications of lack of fusion

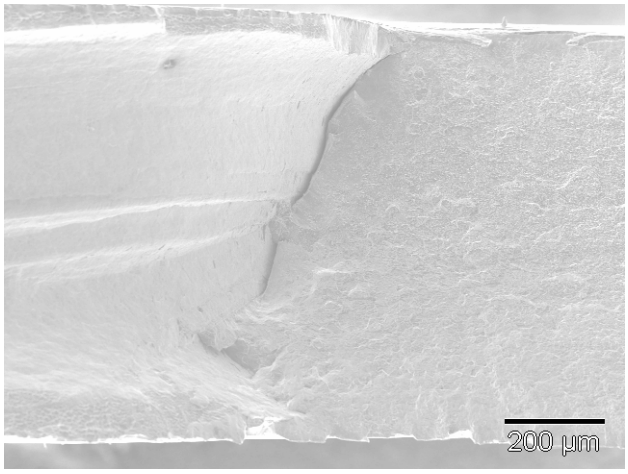

Figure 13: Tensile tested specimen 8 at 100x. Implication of lack of fusion

2. Laser Additive Manufacturing

The additive manufacturing process such as Laser Additive Manufacturing (LAM) is also an important processing tool for Air Force repair and manufacturing applications. For critical components it is vital to understand the mechanical behavior and characteristics of the Heat Affected Zone (HAZ) located in the region between the substrate and the deposit. Process parameters such as heat treatment and Hot Isostatic Press (HIP) procedures determine the local mechanical behavior of the material on a grain scale, control the local residual stress field, and determine the size and frequency of inclusions such as lack of fusion and porosity.

Ti-6Al-4V was the material used for the material investigation. NDI was performed on several sets of material in order to choose a suitable set of materials for testing. Material set B27 was chosen to be used for fatigue and shear testing, while material set B39 was chosen for compact tension testing for crack propagation in the region.

Initial fatigue testing showed failure in the grip section of the fatigue specimen near 5e5 cycles, where life prediction has predicted the material to fail near 1e4 cycles. The fatigue failure occurring outside the gage section of the specimen was of concern, and further specimens were machined to repeat the fatigue testing.

An Iosopescu shear fixture was determined to be the optimal choice for experimentally determining the shear performance of the material along the interface, and to obtain the shear Modulus, G. Finite Element Analysis was conducted for the shear specimen to determine the specimen shape and size necessary to properly test in the 10kip shear testing fixture. Care was taken to ensure that the shear stress variation was minimized in the notched area of the test specimen.

C-T specimens were also designed and machined to determine the mode I crack growth behavior of the LAM process in the HAZ interface region. Special fixture modifications were manufactured in order to use current crack growth testing setup with the designed shapes and sizes. The testing will be performed by David Mahaffey of AFRL/MLLMP of the processing section. The crack growth, shear and fatigue results will be used to develop a comprehensive process performance model for the additive manufacturing process.

3. Material Characterization Study

Poly-crystalline materials under load exhibit varying local strain behavior based on the grain properties themselves, as well as the interaction between each grain. Various deformation mapping techniques can be used to determine the mechanical properties such as modulus based on each grain orientation. A considerable effort has been invested to obtain accurate material properties using experimental and analytical techniques.

Materials with larger grains, such as gamma titanium aluminide, can be instrumented with strain gages on each grain. The results from tensile tests along with Finite Element Analysis (FEA) can be used to predict the Young's modulus for a given orientation. Deformation mapping can produce a more detailed strain distribution for each grain in a polycrystalline microstructure. In addition to using the results to obtain the modulus based on orientation, the strain field results can also locate the position, size and the magnitude of the strain concentrations near the grain boundaries from the grain misorientation. The combination of the results can be used to develop, enhance and validate modeling of polycrystalline materials.

Various experimental techniques can be used to obtain images to calculate full field displacement and strain fields. Subsequent deformation mapping of the images can be used to determine such mechanical properties of many materials and components regardless of size scale. Materials such as Ti-15-Al-33Nb(at.%) have a significantly smaller microstructure than gamma titanium aluminide, therefore strain gages can not be used to characterize each grain's strain. Deformation mapping on a small scale is an application that can be used in this case to characterize the local mechanical, tensile and creep behavior of the material.

The experimental investigation presented here employs a tensile testing stage mounted in a Scanning Electron Microscope (SEM) chamber (Figure14). The images from the SEM are collected for a given area of interest (Figure 15). The tensile stage is stopped at each load level in order to obtain an image. Digital image correlation is conducted on the captured images to obtain the displacement field for the area of interest. An overlay of the strain field (ε_{xx}) on the SEM image for a load of 814Mpa is shown in Figure 16. The loading is in the horizontal (x) direction and the strain field shows the strain concentration forming near the $\alpha 2$ (hexagonal close packed) and β (body-centered cubic) phase boundary.

The orientation of each grain is also important for this particular application in addition to the deformation. Electron Backscatter Diffraction (EBSD) can also be used in the SEM chamber to determine the orientation of a poly-crystalline grain in the region of interest. The tensile stage is also equipped with a heating element that is used to characterize the effect of temperature on the deformation field. The combination of the obtained orientation, temperature control and displacement map from the tensile experiments can also be used to obtain the mechanical property of each grain and to validate mechanical models of the grain interactions on a sub-micron scale.

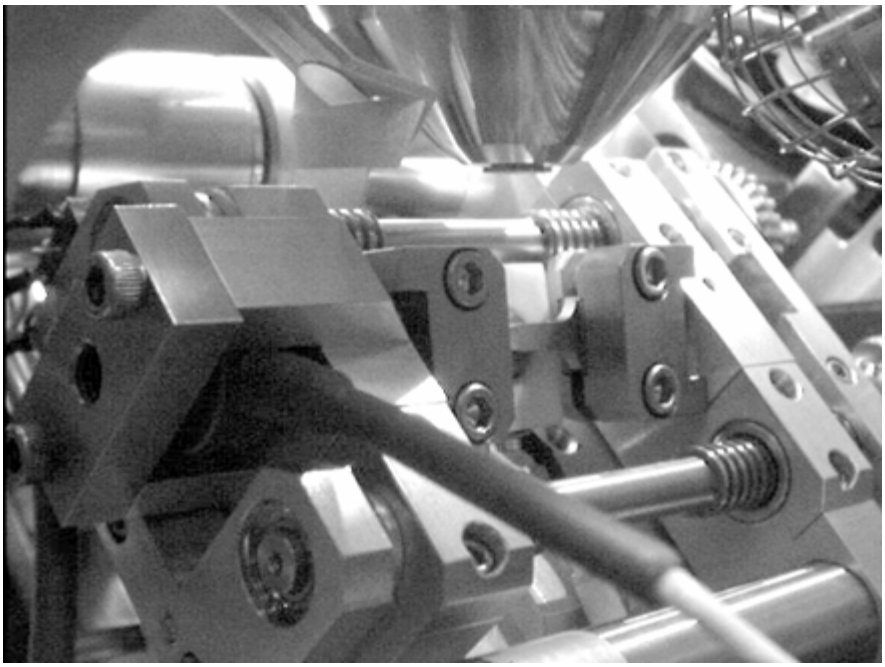

Figure 14: SEM in-situ tensile stage setup.

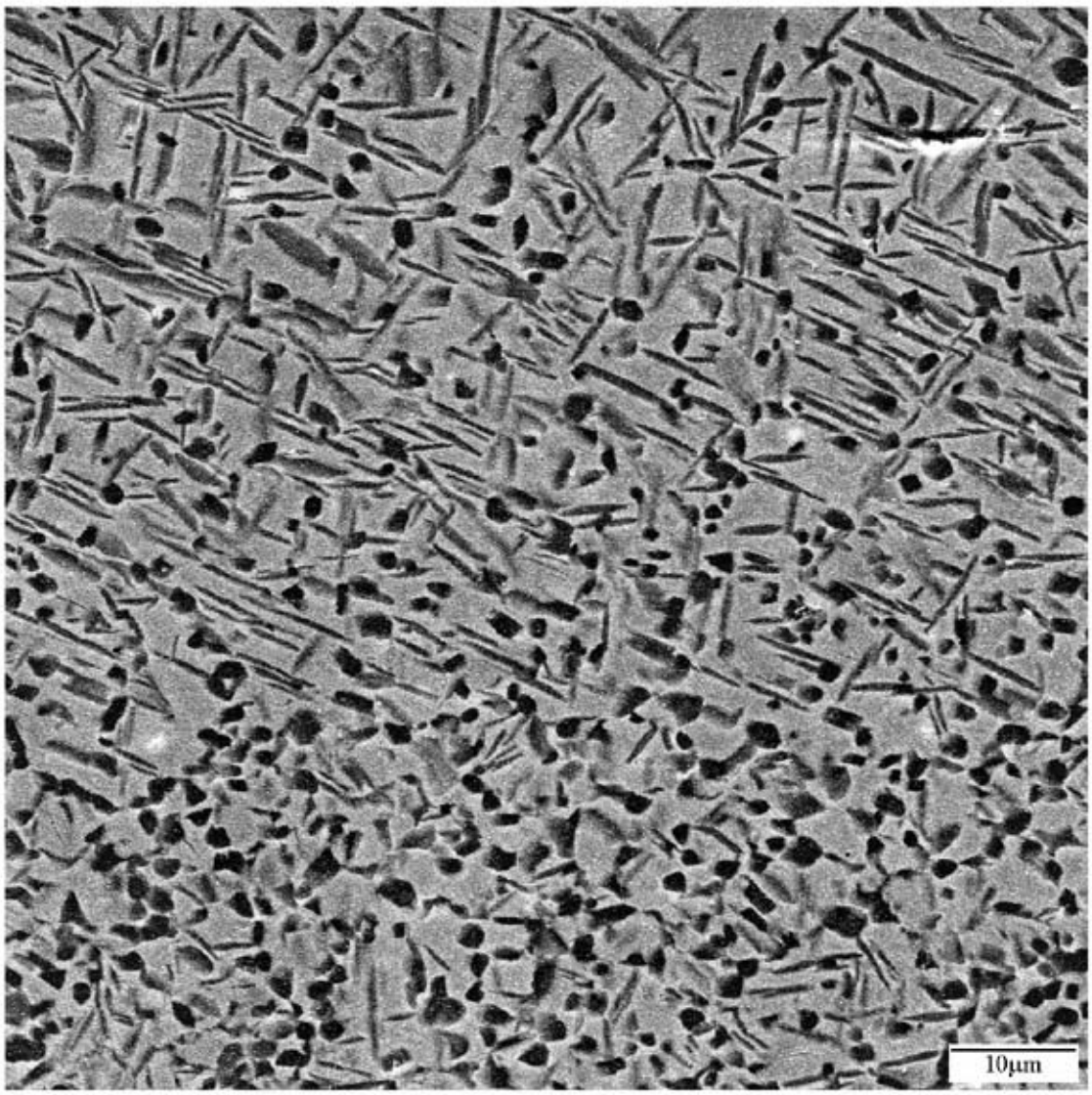

Figure 15: SEM image of area of interest used in deformation mapping

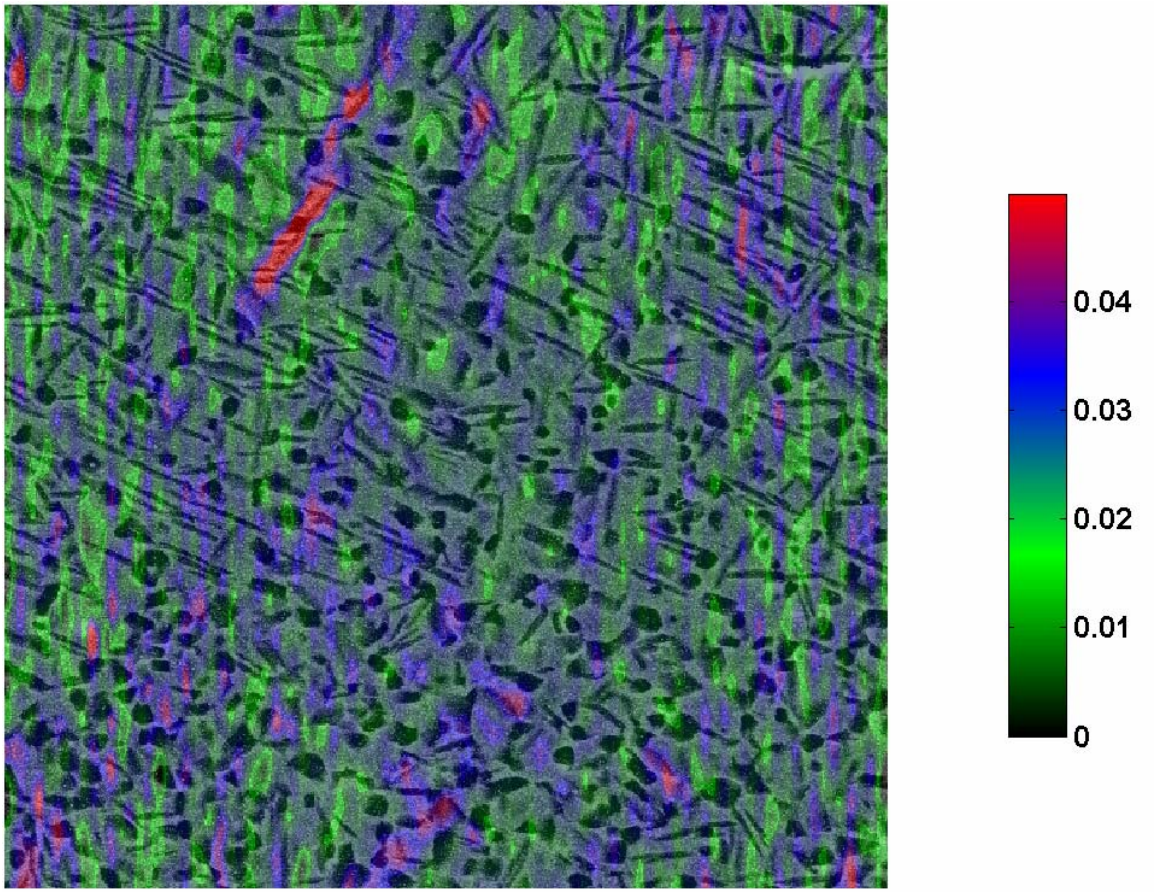

Figure 16: Strain distribution ε_{xx} of Ti-15Al-33Nb at 814MPa

Obtaining the strain field from in-situ testing is not feasible at this point for materials such as Rene 88DT where the material exhibits contrast between grains, but not inside each grain itself (Figure 17). The natural features imaged in each material determine whether a coating is needed to obtain the proper contrast pattern for the imaged area in order to be able to perform digital image correlation. Etching techniques have shown to work with materials such as Gamma Titanium, and displacement maps have been successfully obtained with the aid of optical microscopy.

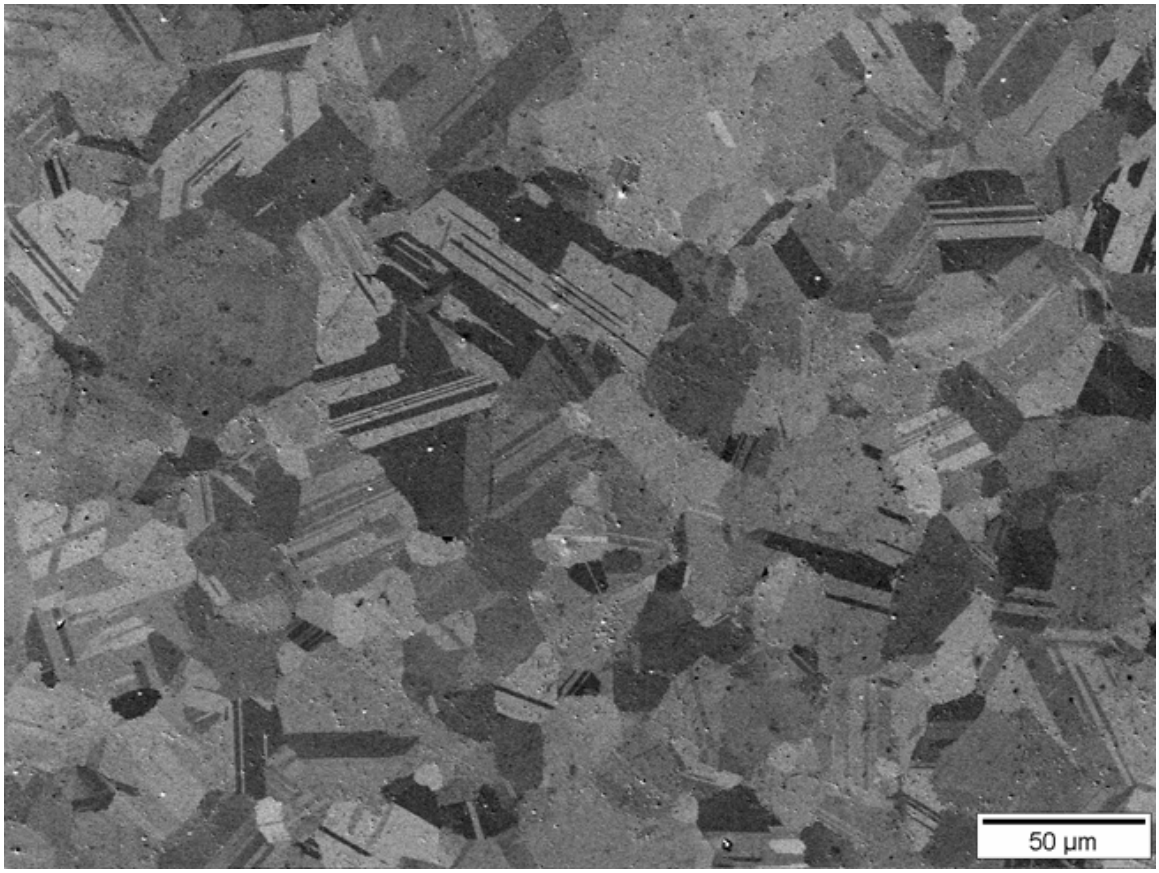

Figure 17: SEM image of Rene 88DT sample.

A tensile test was also conducted at room temperature in-situ inside an SEM. While displacement mapping could not be performed on the secondary or backscatter image, the EBSD of an area of interest was taken before load (Figure 18) and near yield loading (Figure 19). The inverse pole figures show twins appearing inside various grains on the surface. These twins did not disappear upon unloading, and no further twins developed when the test was taken well beyond the yield level of the material.

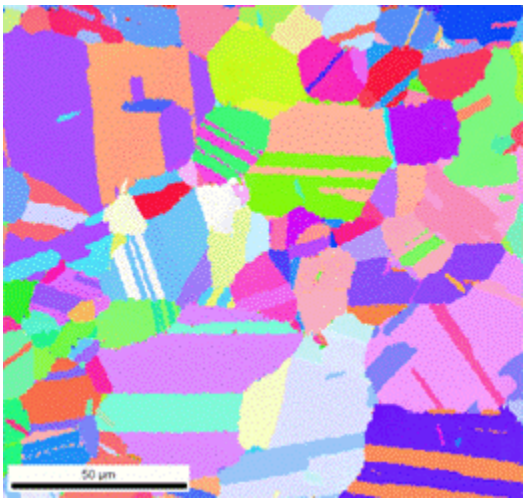

Figure 18: Inverse pole figure of underformed area of Rene 88DT

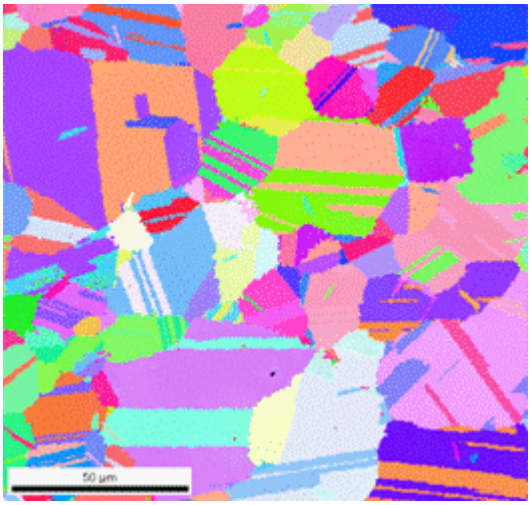

Figure 19: Inverse pole figure showing twins develop near yield.

An optical microscopy technique developed by David Johnson was used to obtain a displacement and a strain field of Rene 88DT that could not be obtained using SEM techniques. A microscope with a CCD digital camera attached to a laptop was used to capture surface images of deformed grains for increasing load steps (Figure 20). The load was applied with a servo-hydraulic MTS testing machine.

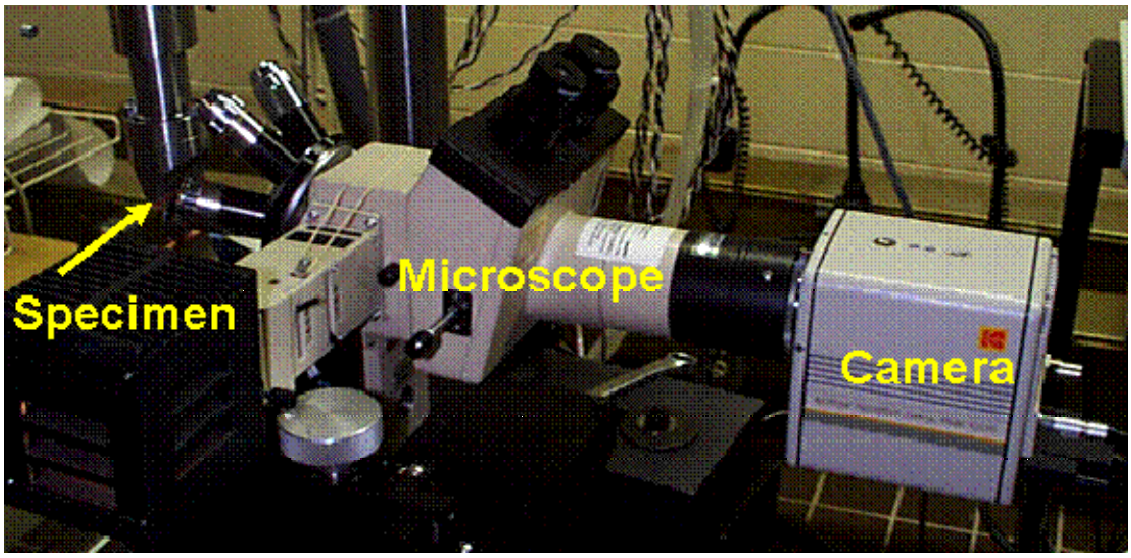

Figure 20: Optical Microscopy Experimental Setup

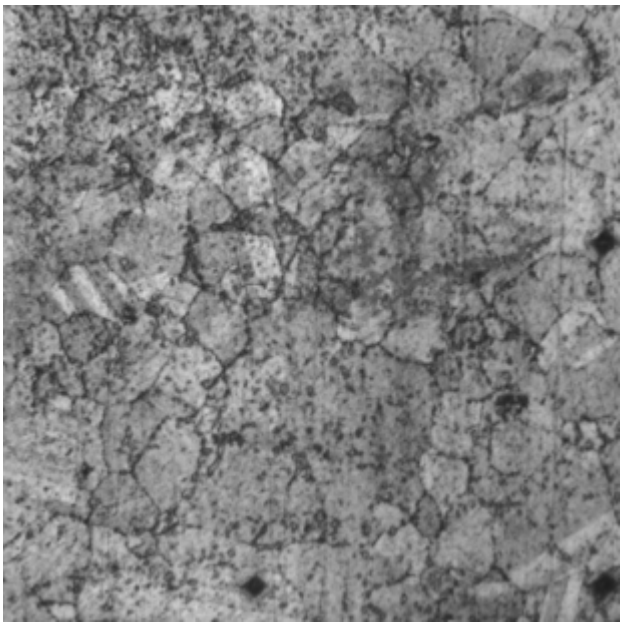

Figure 21: Digital image of the etched surface of Rene 88DT showing fiducial marks.

The surface was prepared with an etchant in order to bring out contrast near each grain boundary and inside each grain. Fiducial marks in the form of Vickers indents were also placed on the surface in order to properly mark the area of interest and to aid in combining displacement and orientation data at the end of the experiment (Figure 21).

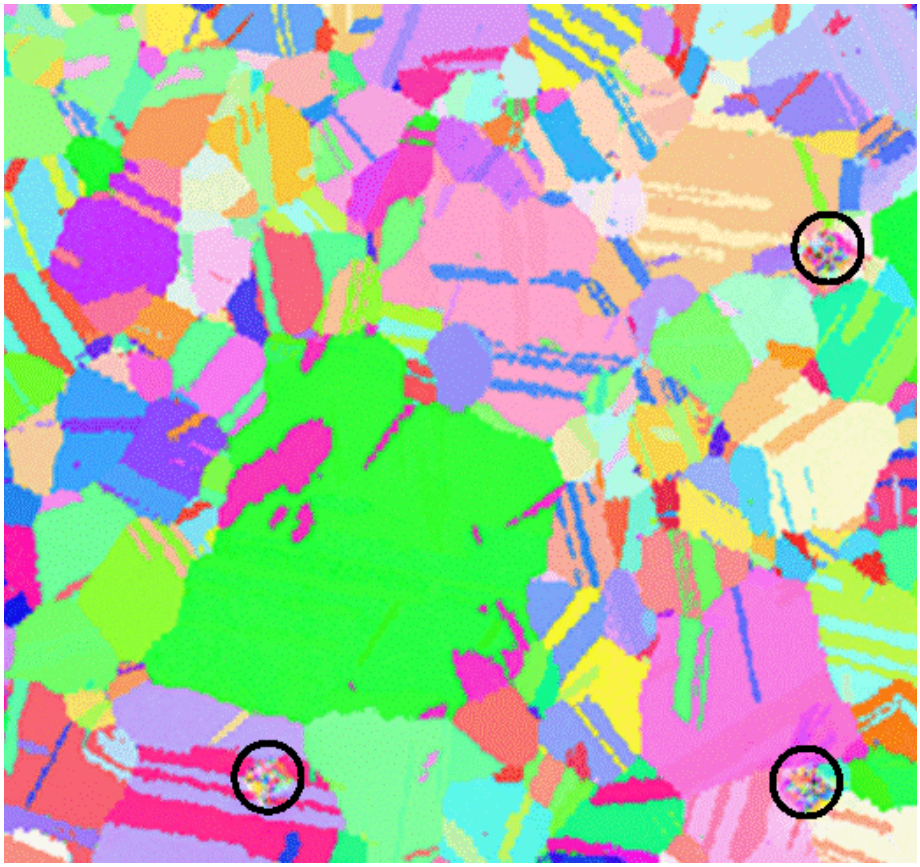

Figure 22: Inverse pole figure of Rene 88DT showing imaged region with fiducial marks.

After the surface was prepared, EBSD map was taken of the specimen surface using a SEM. The indents can clearly be seen in Figure 22. A strain gauge was next mounted on the back side of the specimen for calibration purposes, and the specimen was mounted into a servo-hydraulic machine. An image of the area of interest was taken at specific load levels throughout the tensile test. The test was interrupted for each load step in order to position and focus the image properly for strain mapping. The test was in displacement control changing the voltage in order to increase the strain of the specimen.

Vic-2D was used in order to calculate the displacement of the pixels relative to lower load steps. The unreformed image was also aligned in Figure 23 with the grain boundary data obtained from EBSD in order to obtain the grain number, Euler angle, displacement, and strain distribution

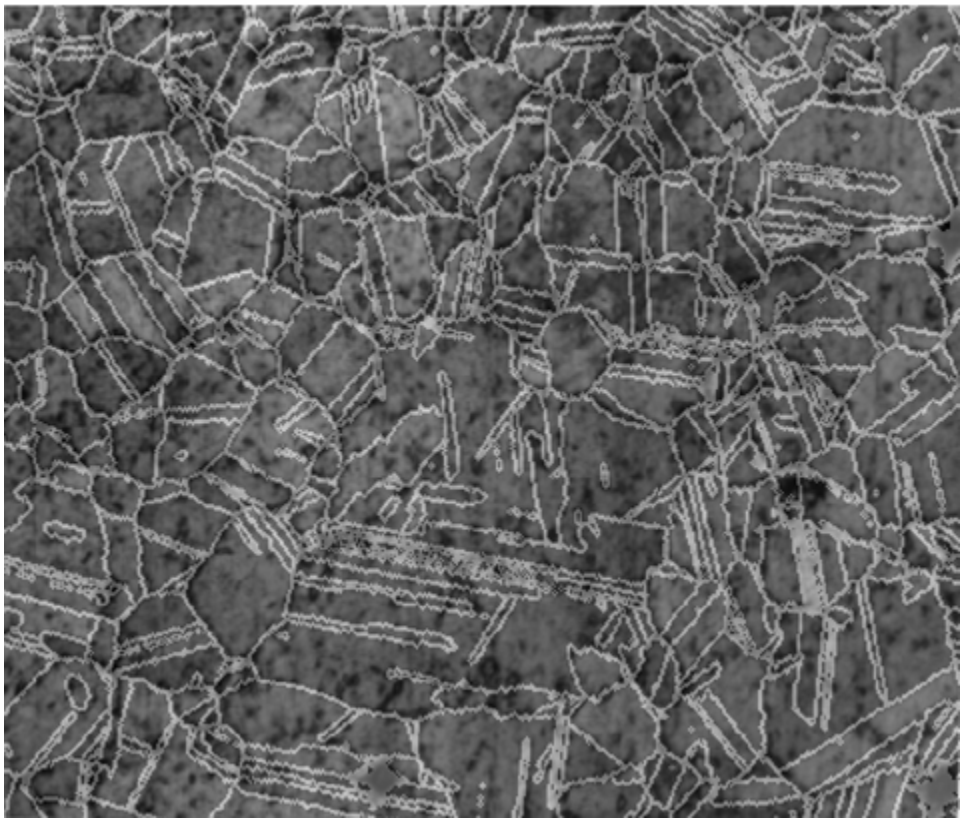

Figure 23: Optical image aligned with grain boundary data obtained from EBSD.

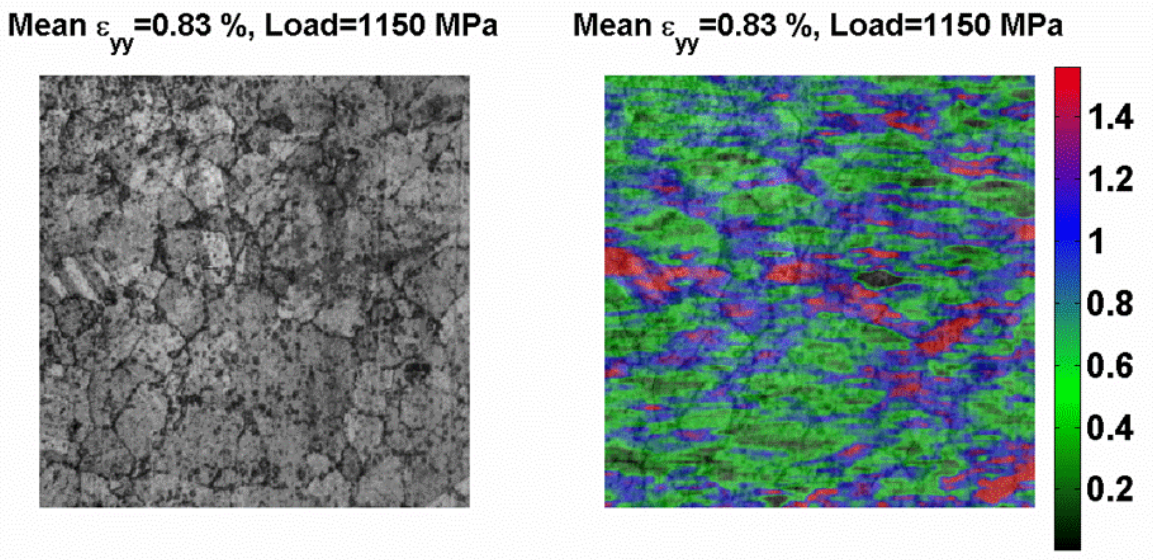

Figure 24: Deformed optical image and strain map overlay near yield. Strain concentrations develop near large grain boundary.

The results show the heterogeneous behaviour of larger grains in the plastic regime (Figure 24). The difference in the stress-strain behavior can be attributed to grain size, orientation, and grain interactions (Figure 25). Further modelling is needed in order to determine the importance of each variable on the crystal plasticity behaviour of the material.

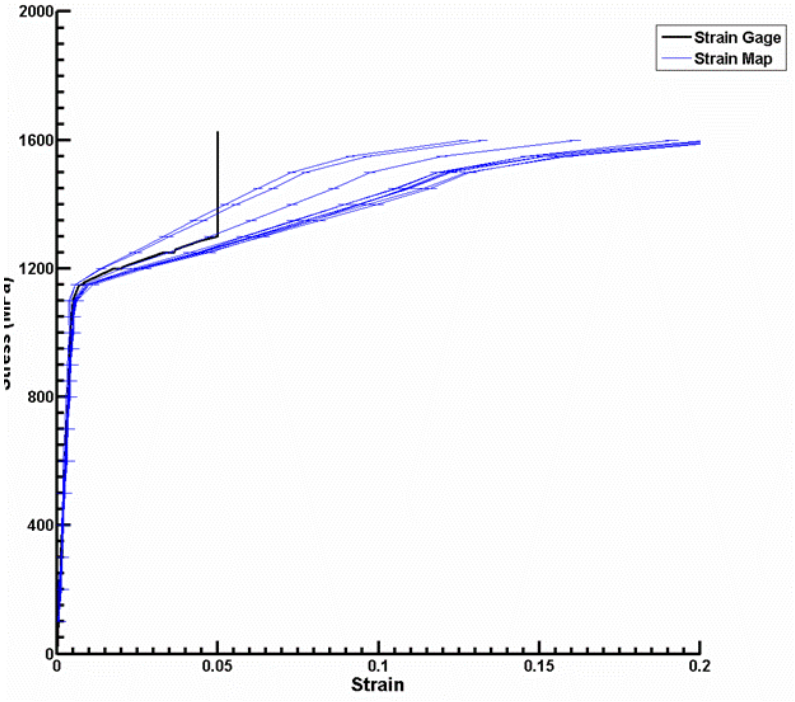

Figure 25: Stress strain curve for the mean strain of grains larger than 15μm^2 area.

4. Contact Mechanics Study

Several Various journal publications have been submitted and published over the course of last year using developed elasticity based contact mechanics programs in conjunction with stress based life prediction tools. The journal publications deal with the experimental and the computational side of contact mechanics, validating and developing contact mechanics and life prediction tools associated with contact fatigue.

Bartha, B. B, Nicholas T, Farris, T.N., Contact Analysis of Relatively Thin Elastic Layers, *Journal of Strain Analysis*, Submitted, April 2006

Golden, P. J., Hutson A. L., **Bartha, B. B.**, Nicholas, N., Comparative Testing and Analysis of Fretting Fatigue Test Fixtures, *Experimental Mechanics*, Submitted, December 2005

Garcia, D. B., Grandt Jr., A. F., **Bartha, B. B**., Golden, P. J., Threshold Fatigue with Fretting Induced Cracks in Ti-17, *Engineering Fracture Mechanics*, Submitted, October 2005

Bartha, B. B, Nicholas T, Farris, T.N., Geometry Effects in Fretting Fatigue , High Cycle Fatigue a Mechanics of Materials Perspective, Elsevier, In Press, June 2006

Bartha, B. B, Nicholas T, Farris, T.N., Modeling of Geometry Effects in Fretting Fatigue, *Journal of Tribology*, In Press, June 2006

5. Summary

The current task developed various experimental and computational tools to determine the material behavior of weld interfaces and local grain behavior of materials. Stereo imaging, optical microscopy and scanning electron microscopy were used to determine the local interfacial characteristics of welds as well as microstructural characteristics of grains at a micro-scale. Computational tools were developed to analyze and combine the tensile and fatigue data for the various applications. The data shows large strain concentrations develop near the weld interface develop for resistance welds, and near grain boundaries of grain interfaces. The combined data shows the heterogeneous behavior of grains on a micro-scale. Further crystal plasticity and process performance models are needed t characterize the intrinsic material behaviors that are seen for the particular set of materials and boundary conditions. Semi-analytical computational tools that determine the stress field of two contacting bodies were also used to analyze and publish data for various contact fatigue applications. The results in the publication show the need for accurate stress based modeling tools to predict the fatigue and crack growth behavior of contacting bodies.